Nuclear Engineering and Technology 53 (2021) 2909–2917

Contents lists available at ScienceDirect

Nuclear Engineering and Technology

journal homepage: www.elsevier.com/locate/net

Original Article

Design of muon production target system for the RAON μSR facility in Korea

Jae Young Jeong [a], Jae Chang Kim [a], Yonghyun Kim [a], Kihong Pak [a], Kyungmin Kim [a], Junesic Park [a], Jaebum Son [a], Yong Kyun Kim [a, *], Wonjun Lee [b], Ju Hahn Lee [b]

[a] Department of Nuclear Engineering, Hanyang University, Seoul, 04763, South Korea
[b] Institute for Basic Science (IBS), Daejeon, 34047, South Korea

ARTICLE INFO

Article history:
Received 24 November 2020
Received in revised form
1 March 2021
Accepted 26 March 2021
Available online 10 April 2021

Keywords:
Proton interaction
Muon facility
Muon production target
Surface muon
Rotating target
Monte Carlo simulation

ABSTRACT

Following the launch of Rare Isotope Science Project in December 2011, a heavy ion accelerator complex in South Korea, named RAON, has since been designed. It includes a muon facility for muon spin rotation, relaxation, and resonance. The facility will be provided with 600 MeV and 100 kW (one-fourth of the maximum power) proton beam. In this study, the graphite target in RAON was designed to have a rotating disk shape and was cooled by radiative heat transfer. This cool-down process has the following advantages: a low-temperature gradient in the target and the absence of a liquid coolant cooling system. Monte Carlo simulations and ANSYS calculations were performed to optimize the target system in a thermally stable condition when the 100 kW proton beam collided with the target. A comparison between the simulation and experimental data was also included in the design process to obtain reliable results. The final design of the target system will be completed within 2020, and its manufacturing is in progress. The manufactured target system will be installed at the RAON in the Sindong area near Daejeon-city in 2021 to carry out verification experiments.

1. Introduction

In the field of matter science, the applications of surface muons, i.e., positively charged spin-polarized muons, have been studied since muons were discovered by Carl D. Anderson and Seth Neddermeyer at Caltech in 1936 [1]. Surface muons play an important role in the muon spin rotation, relaxation, and resonance (μSR) techniques. The distribution and dynamics of nuclear and atomic magnetic fields in matter can be studied from the decay of surface muons. Owing to their significant role in condensed matter physics, the demand for muon facilities has been continuously increasing. Currently, there are several muon facilities worldwide that produce surface muons, such as Paul Scherrer Institute/SμS(Switzerland) [2], J-PARC/MUSE(Japan) [3], RCNP/MUSIC(Japan) [4], TRIUMF/CMMS(Canada) [5], and ISIS Neutron and Muon Source (UK) [6]. Additionally, China and the USA are constructing and planning to build new muon facilities. In South Korea, the Rare Isotope Science Project was launched in December 2011, and a heavy-ion accelerator complex, named RAON, was designed, including a muon facility for μSR.

The target system for the muon facility in RAON aims to induce the production of a significant amount of surface muons in thermally stable experiments. In this design, the target shape and operation method were determined by considering the following requirements.

- The proton–nucleus interaction length should be significantly long.
- The coolant safety management should be easy.
- The target should not interfere with the direction of the secondary particles for beamline extension.

To satisfy the above requirements, a new target system was proposed.

The superconducting linear accelerator at RAON will be able to accelerate a proton beam with an energy up to 600 MeV and currents ranging up to 660 μA. The full width at half maximum of the proton beam in the X and Y directions is 2.7 mm and 6.75 mm, respectively, at the target position [7]. The μSR facility will be operated with a 40 kW proton beam in the early stage of operation,

* Corresponding author.
E-mail address: ykkim4@hanyang.ac.kr (Y.K. Kim).

https://doi.org/10.1016/j.net.2021.03.023

and the power of the proton beam is expected to ramp up to 100 kW. We designed the target system to produce a sufficient amount of surface muons using a 40 kW proton beam. Furthermore, thermally stability must be guaranteed during a collision of the 100 kW proton beam, which has the highest beam power in the early stage.

In Section 2, the target design process is described. It entails target material selection, target size determination, and estimation of the surface muon yield with the determined target. In particular, surface muon yield estimation was performed by comparing the simulation results from the Geant4 toolkit [8] to the previous study in Paul Scherrer Institute (PSI). Section 3 describes the entire target system, i.e., the configuration for the target system and a discussion of its thermal analysis result.

2. Target design

Target design was carried out using the procedure described in Fig. 1.

First, the target material was selected in accordance with the surface muon yield and material properties. Next, three design criteria were set: surface muon yield, maximum temperature, and maximum stress. The design was performed through an optimization process. At the beginning of optimization, the concept of the target such as shape and operation of the target was determined. Thereafter, the thickness of the target was optimized by considering the correlation between the proton beam and thickness. The radius and rotational speed of the target, which mostly affect the target thermal stability, were optimized through thermal analysis using MCNP and ANSYS. After determining the target dimension, the surface muon yield was calculated using Geant4. In order to produce reasonable results from simulations, it is necessary to select an appropriate physics model for describing the proton-nucleus interactions as accurately as possible, especially in terms of the surface muon yield. We selected one appropriate physics model by comparing the PSI data with the calculation results among three physics models embedded in Geant4: QGSP_BERT, QGSP_BIC and QGSP_INCLXX. After selection of the physics model,

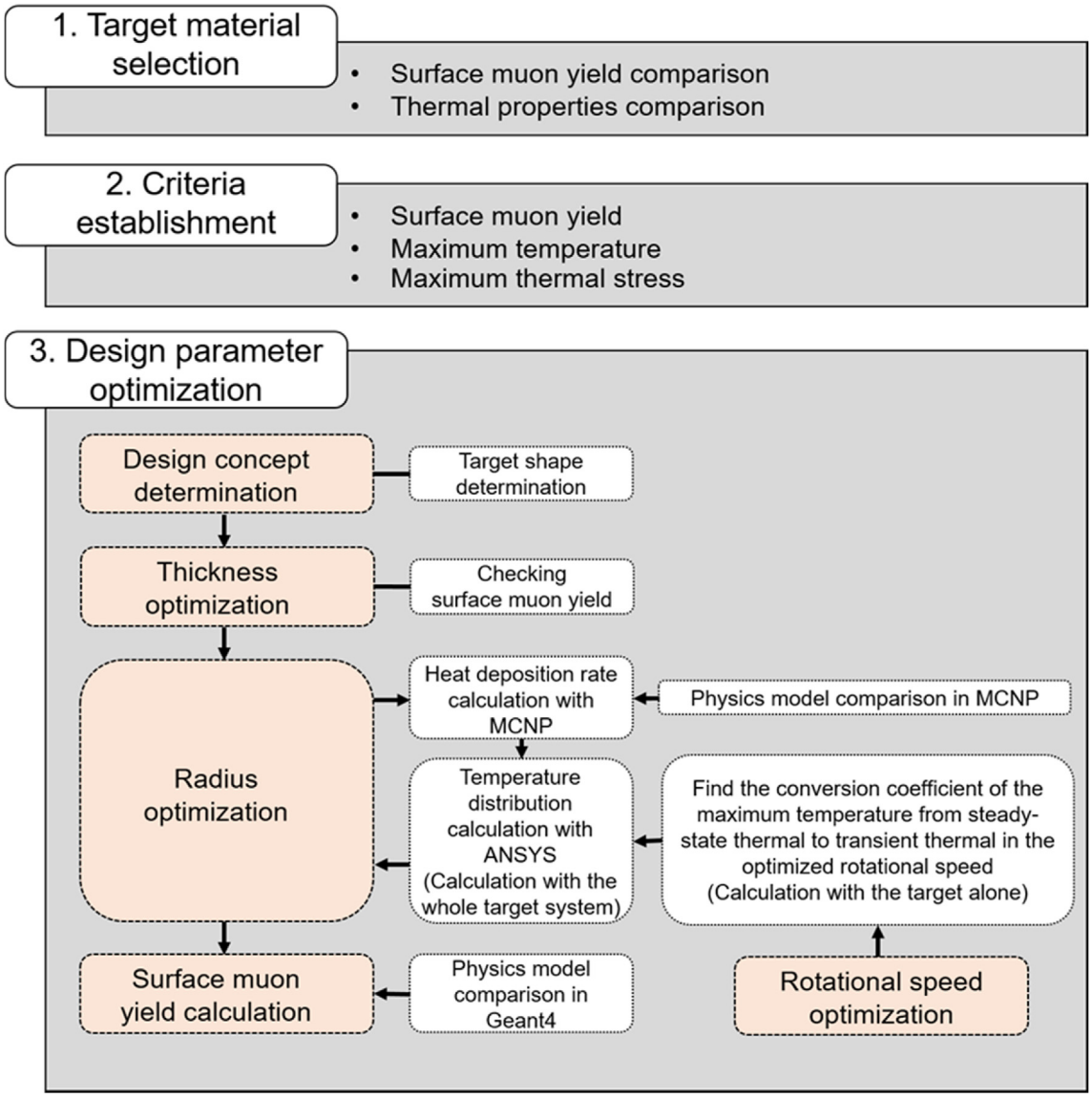

Fig. 1. Procedure of μSR target design.

it was verified whether the designed target satisfies the surface muon yield criterion.

2.1. Material selection

Surface muons are produced by nucleus-nucleus interactions. When the target is bombarded with high-energy protons accelerated from the superconducting linear accelerator, various secondary particles, including positive pions, are produced from the proton–nucleon reactions. A surface muon is a 100% polarized muon produced by the decay of a positive pion at rest on the surface of the target. To induce the above interaction, it is advantageous that the target consists of low-atomic-number materials, such as graphite and beryllium.

The surface muon target was determined by considering both the surface muon yield and material properties. As for the surface muon target, the following three materials were considered: polycrystalline graphite, boron nitride (BN), and boron carbide (B_4C). These materials have been widely studied for the muon production target. Among the various polycrystalline graphite candidates, IG-4.

30U made by Toyo Tanso Co., Ltd. was chosen, which has proven useful in J-PARC/MUSE [9,10]. The material properties of these target candidates are listed in Table 1 [11,12]. The muon yield comparison was performed using the Geant4 simulation with the geometry condition described in Fig. 2. As shown in Fig. 2 and 600 MeV protons were bombarded with the box-shaped target. Surface muons with momentum ranging from 27.5 to 29.5 MeV/c were counted at the 25 cm radius muon detector position, and the surface muon yield with each material is shown in Table 2.

B_4C has the highest density and physical strength, but its thermal conductivity and melting temperature are significantly lower than the other candidates. In contrast, polycrystalline graphite (IG-430U) has the highest melting point and thermal conductivity. Moreover, the simulation results demonstrated that the number of counted surface muons in the interaction with protons and IG-430U was comparable to that of B_4C. In terms of surface muon yield alone, B_4C is a desirable choice. However, the yield difference is not as large as that of polycrystalline graphite, which has a better thermal stability than the rest of the candidates. Therefore, IG-430U was chosen as the target material because it was believed that thermal stability is more important than the few yield differences mentioned above.

2.2. Criteria establishment

In typical μSR experiments, the time window of the μSR signal extends to approximately 5 muon lifetimes, such as 10 μs This indicates that at least 10^5 surface muons per second are required for μSR experiments. The criterion for surface muon yield was determined to be 2×10^7 per second with a 40 kW proton beam, considering the minimum transmission rate and margin.

Even though the melting point of graphite is 3407 °C, which is quite high compared to the other materials, the maximum target temperature criterion was determined based on the evaporation point. According to a 2002 report [13], when the surface temperature of graphite was approximately 1850 °C at 10^{-6} Torr, it showed a sufficiently small sublimation rate of 2.2 μm/day. Therefore, the temperature criterion was determined to be 1531 °C, which has a 15% safety margin for the simulation error and temperature change due to an unexpected accident. The thermal stress criterion was determined to be half the tensile strength of IG-430U. The target design criteria are shown in Table 3.

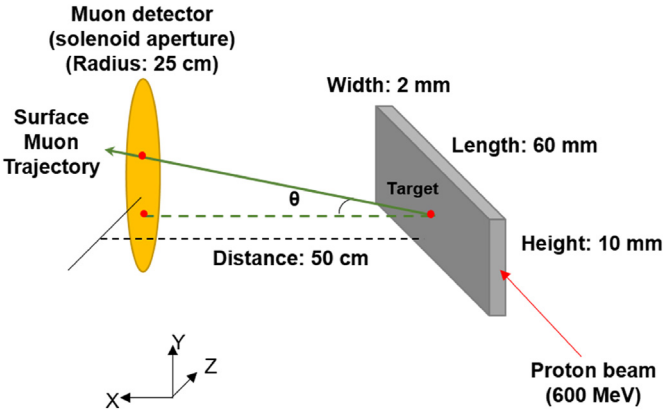

Fig. 2. Geometry condition for Geant4 simulation for material selection.

Table 2
Surface muon yield for each material with a 40 kW proton beam.

	Graphite	B_4C	BN
Surface muon yield (#/sec)	8.167×10^9	8.631×10^9	7.920×10^9
Standard deviation (#/sec)	9.037×10^4	9.290×10^4	8.900×10^4

2.3. Design parameter optimization

2.3.1. Design concept determination

Because the muon is produced using a high-power beam, the thermal damage to the target should be minimized to perform a stable experiment. Instead of cooling the target directly, the rotating target is cooled by distributing the beam evenly over the target and selecting a material with high thermal conductivity and thermal emissivity as the target material. Manufacturing the rotating target involves technical difficulties, such as the lifespan issue, owing to rotating parts in a high-radiation environment. However, it has advantages in safety management, that is, prevention of accidents, such as activated coolant leakage. The suggested method of colliding the proton beam on the rotating target is shown in the conceptual diagram in Fig. 3.

The proton beam will collide with the disk-shaped target from the side for maximum interaction with the target. The disk shape is suitable as a simple target shape that does not interfere with the direction of secondary particles. As the disk-shaped target rotates, the generated heat is dissipated in an annular form, and secondary

Table 1
Material properties of target material candidates.

Product	Bulk Density (g/cm^3)	Tensile Strength (MPa)	Compressive Strength (MPa)	Young's Modulus (GPa)	Coefficient of Thermal Expansion (10^{-6}/K)	Thermal Conductivity (W/(m·K))	Melting Point (°K)
Graphite (IG-430U)	1.84	56.8	99	10.8	5.2	140	3773
B_4C	2.3–2.55	261–569	2583–5687	362–472	3.2–9.4	17–42	2645–2780
BN	1.9–2.3	27–83.3	224–540	19.5–100	1–6	19–52	3150–3400

Table 3
Target design criteria in surface muon yield, maximum temperature, and maximum stress.

	Surface muon yield with a 40 kW proton beam (/sec)	Maximum Temperature (°C)	Maximum Stress (MPa)
Criterion	2×10^7	1531	28.4

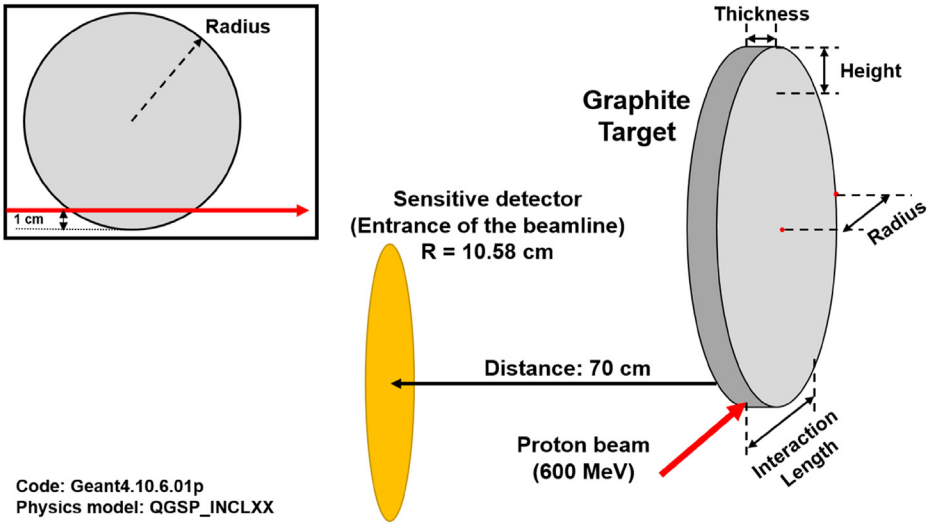

Fig. 3. Conceptual diagram of the beam irradiation method for the disk-shaped target.

particles can be emitted in all directions except in the top direction. This concept can be used to change the deposited heat and the surface muon yield by adjusting only the vertical position of the target.

2.3.2. Thickness optimization

The thickness of the target is an important factor in the surface muon yield because of the short total range of the surface muons (~140 mg/cm^2). The thickness of the target was determined by considering the size of the proton beam, surface muon yield, and mechanical issues. Fig. 4 shows the surface muon yield per 10^9 protons with various target thicknesses and beam sizes, calculated using Geant4 under the conditions described in Fig. 3.

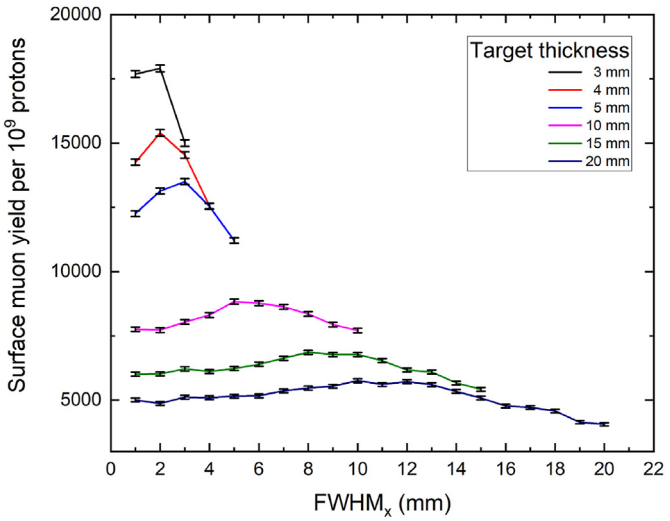

Fig. 4. Surface muon yield per 10^9 protons with various target thicknesses and beam sizes.

Fig. 4 shows that the target thickness has an optimal value depending on the beam size according to the surface muon yield. Furthermore, it shows that the thinner the target, the higher the surface muon yield. This result is in good agreement with the data reported in 2015 [14]. However, when the target becomes significantly thin, it can cause unexpected fractures and breakage owing to cracks. Moreover, even if there is a small proton beam misalignment, the proton beam can hit the beam dump directly without passing the target. Therefore, the thickness of the target was determined to be 5 mm, considering the surface muon yield and the safety margin for the proton beam misalignment. The surface muon yield for the determined thickness was the highest when the full width at half maximum (FWHM) of the proton beam in the X direction was 2.7 mm.

2.3.3. Radius optimization

The target radius is closely related to heat stress, costs, and the amount of radioactive waste. The target radius was determined to satisfy the criteria through ANSYS thermal analysis with a 100 kW proton beam. The heat deposition rate for thermal analysis was derived by MCNP6.1 [15], which is considered to be the most accurate for the transport of protons and neutrons. In MCNP simulations, the target was separated into cylindrical meshes, and the heat deposition rate for each mesh was derived by mesh tally. To obtain conservative result, CEM03/GEM model was applied, which shows 5–9% high heat deposition rate than the other physics models.

Fig. 5 shows the maximum temperature as a function of rotational speed calculated with transient thermal (TR) and steady-state thermal (SS) methods for the 20 cm radius target. The chamber design was not considered in these calculations, i.e. calculation without chamber. The maximum temperature of the target decreases rapidly when the rotational speed increases from 0 to 5 rpm. After the rotational speed exceed 5 rpm, the maximum temperature decreases slowly. And then, the TR calculation and SS calculation are approximately the same at 30 rpm and above.

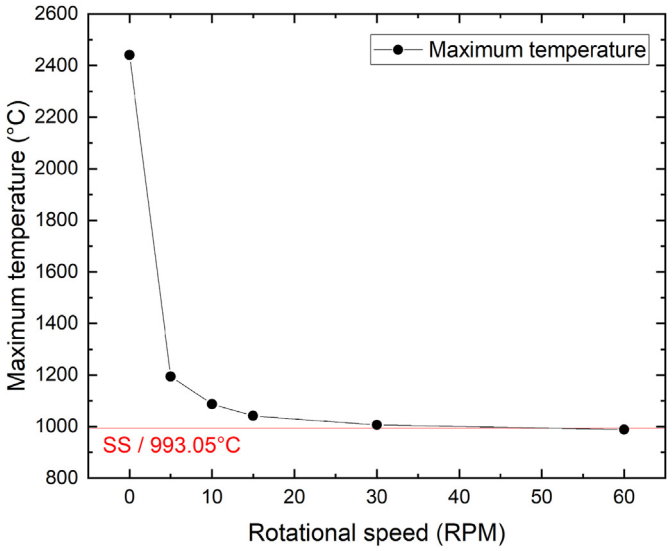

Fig. 5. Transient thermal (TR) and steady-state thermal (SS) calculation results by the six rotational speeds for the target of 20 cm radius without chamber.

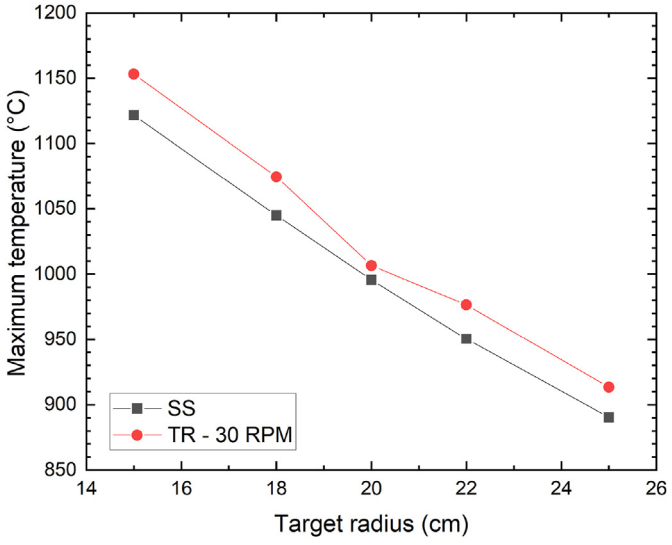

Fig. 6. Maximum temperature comparison between SS calculation and TR calculation at 30 rpm rotational speed for targets of five radii without chamber.

Therefore, the rotational speed of the target was determined to be 30 rpm or higher. Fig. 6 shows the maximum temperature comparison between the SS calculation and TR calculation at 30 rpm rotational speed for targets of five radii without chamber. The difference between the two calculations for these radii is less than 3%.

Fig. 7 shows the result of the SS calculation in the geometry, including the chamber for each radius of the target. In the case of including the chamber in the calculation, the temperature rise occurs owing to radiation heat returning to the target from the inner wall of the chamber. Considering the temperature rise of approximately 3%, which is a comparison result of TR and SS in the calculation result, the temperature criterion was satisfied when the target radius was 20 cm. If the target radius is larger than 20 cm, the temperature may be lower; however, the amount of radioactive waste can be greatly increased. Therefore, it was determined that the radius of the target was 20 cm.

Fig. 8 shows the results of the thermal stress analysis with a

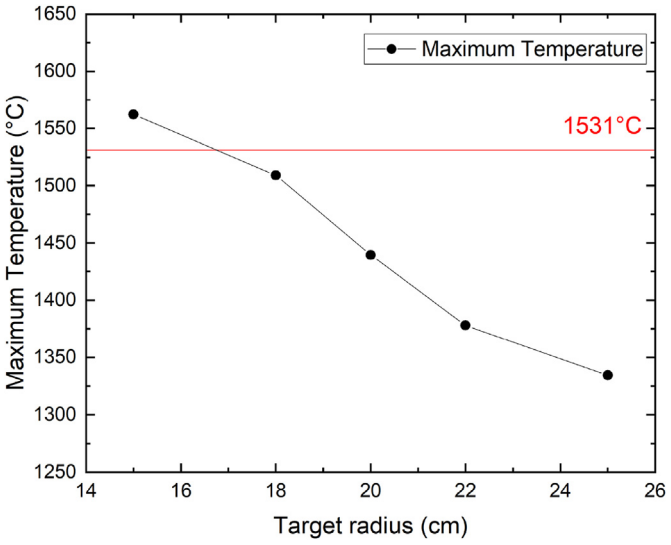

Fig. 7. SS calculation result in the geometry including the chamber for each radius of the target.

100 kW proton beam for the designed target system. A maximum stress of 0.3213 MPa was obtained at the target joint part, which is significantly lower than the stress criterion. To reduce distortion caused by thermal expansion of the target, the target contains 100 mm diameter holes and 3 mm gaps at 120° intervals.

2.3.4. Surface muon yield calculation

The surface muon yield calculation for the designed target system was performed using the Geant4 simulation toolkit. In the calculation, a physics model that can produce the most similar prediction to the actual experimental results was applied. A preliminary simulation was performed to select a suitable physics model among the built-in physics models. The model that showed the most similar results to the PSI data [16] in terms of muon direction and production yield was applied to the calculation.

Three physics models, which are mainly used in the simulation of high-energy proton–nuclear interactions, were applied to the preliminary simulation: QGSP_BERT, QGSP_BIC, and QGSP_INCLXX from Geant4.10.6. p01. As reference data, the data reported by the PSI facility were compared with the results obtained from the above simulation. The simulation conditions and results are shown in Fig. 9 and Table 4, respectively.

QGSP_BERT, QGSP_BIC, and QGSP_INCLXX show an average of 4.653, 0.5772, and 3.432 times higher surface muon yield than the PSI data, respectively. To determine a physics model with the most similar surface muon emission direction trend to the PSI data, surface muon yield at each direction in Table 4 are normalized by total surface muon yield in each physics model, as shown in Fig. 10.

In Fig. 10, the side with the largest surface area shows a higher amount of generation than the rest. QGSP_BERT and QGSP_BIC show more surface muon yield at the forward than at the backward. Conversely, the backward of QGSP_INCLXX has more surface muon yield than the forward, showing the same trend as PSI data. However, QGSP_INCLXX shows a rather low yield ratio on the side. Therefore, the surface muon yield was calculated by applying QGSP_INCLXX and considering the correction factor. The correction factor can be selected between the two cases.

1) Because the direction of the surface muon is the side, the surface muon yield is divided into 2.684 times, which is the difference in the side direction.

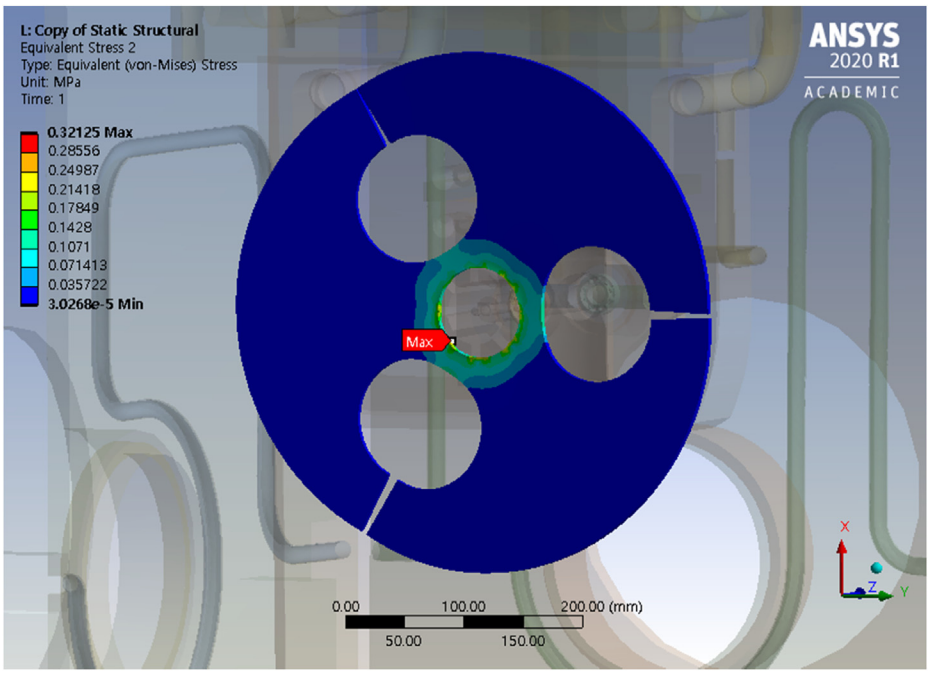

Fig. 8. Thermal stress distribution for the target when 100 kW proton beam colliding.

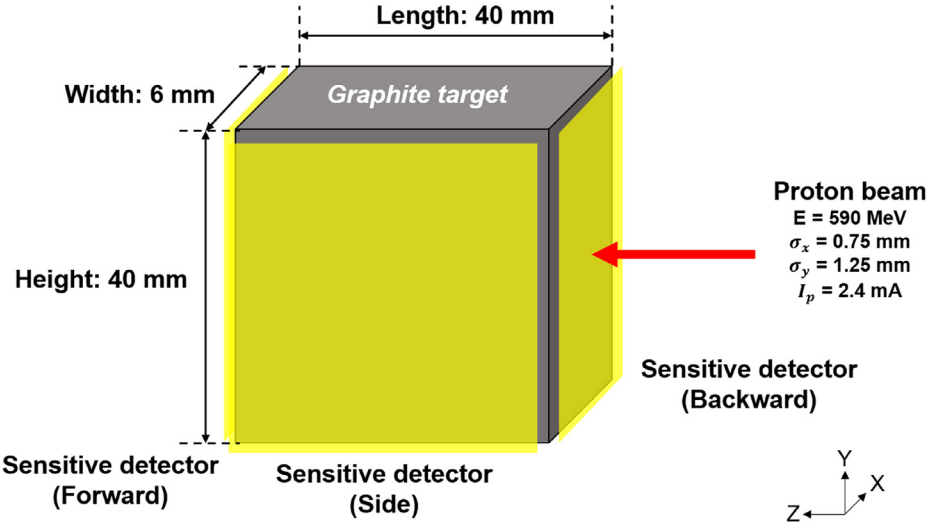

Fig. 9. Simulation condition for comparison between PSI data and our Geant4 simulation results with several physics models.

Table 4
The number of counted surface muons per second at each physics model and direction compared to PSI data.

	Counted surface muons per second ($\times 10^{10}$)			
	PSI data	QGSP_BERT	QGSP_BIC	QGSP_INCLXX
Forward (F)	1.100	7.805	0.8557	4.361
Backward (B)	1.800	6.031	0.8327	6.565
Side (S)	12.00	42.16	5.894	32.21

2) Because the response length is longer than the above simulation, the contribution of forward and backward increases; thus, the surface muon yield is corrected by dividing into 3.432 times, which is the average of the differences in all directions.

We decided to calibrate 3.432 times to obtain a more conservative result.

By applying the simulation conditions in Fig. 3, i.e. the optimized target geometry, and the selected physics model, the simulation was performed to predict the surface muon yield of the designed target. Only the surface muons with a momentum between 27.5 and 29.5 MeV/c and an angle of incidence of 150 mrad or less were counted at the entrance of the beamline based on the acceptance of the beamline. Thus, by applying the correction to the simulation results, 4.736×10^7 surface muons per second could be expected at the entrance of the beamline if a 40 kW proton beam was provided. This is sufficient to satisfy the surface muon yield criterion.

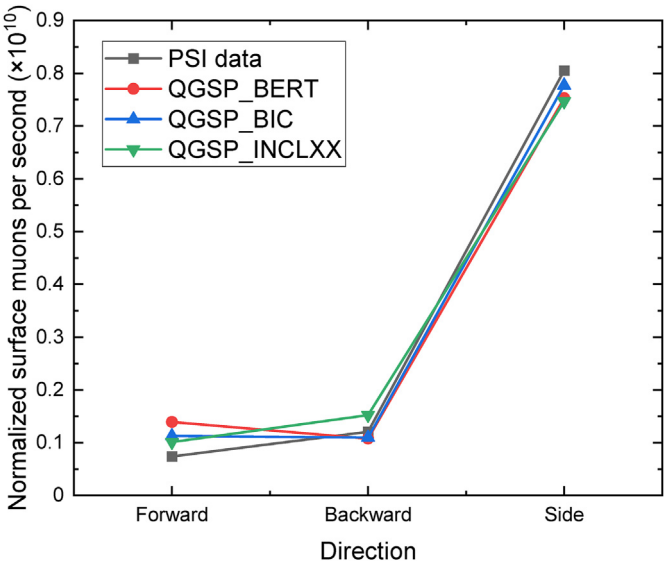

Fig. 10. Surface muon emission direction trend with each physics model.

3. Chamber design

The main considerations of target chamber design were as follows.

- Stable vacuum for high doses and high heat during operation
- Ease of maintenance
- Ease of alignment of the target

The design was carried out in consideration of the above, and safety was verified through MCNP and ANSYS.

3.1. Chamber configuration

The target system can be separated into three parts, as shown in Fig. 11: the target, copper plate, and outer wall parts.

The three-stage separate chamber type is designed such that it separates and repairs only a part of the chamber rather than the entire chamber when a problem occurs at that part of the chamber.

The designed target is combined with the shaft through the target joint. The shaft that receives torque from the motor and the shaft coupled to the target are connected through bevel gears to rotate the target. Because the temperature of the target reaches 1480 °C, we used Ti−6Al−4V, which has a high melting point and high durability for the target joint and shaft in contact with the target.

The motor for rotating the target was attached to the outside of the top of the chamber because inside the chamber it could be damaged by exposure to high doses. In this case, the shaft may penetrate the chamber and damage the vacuum integrity of the chamber. Therefore, a magnetic clutch was attached to the top of the chamber to prevent the shaft from penetrating.

The area close to the target is surrounded by copper plates with cooling water pipes to cool the radiation heat emitted from the target. The rest of the structure is made of SUS304, which has good durability, does not corrode well, and is economical. In particular, the height of the chamber was 3 m tall, and the interior of the chamber was filled with SUS304. Thus, minimizing the neutron dose by keeping the motor and vacuum seal away from the target and placing an SUS304 shield in the middle.

Alignment rails and girders were used to accurately align the target to the desired position.

As shown on the left side of Fig. 12, there are four beam ports on the outer wall of the chamber. Two are ports for the proton beam, and one is facing the direction of the muon transport beamline. The other is a port designed for another surface muon beamline to be constructed in the future, and it will be blocked until construction. Currently, the structure of the target system designed is shown on the right side of Fig. 12.

3.2. Cooling requirement

ANSYS SS calculations were performed to determine the appropriate flow rate of the cooling water flowing through the designed cooling line. As a design criterion, a maximum cooling tube inner surface temperature of 70 °C was used in consideration of the safety margin. The film coefficient (heat convection

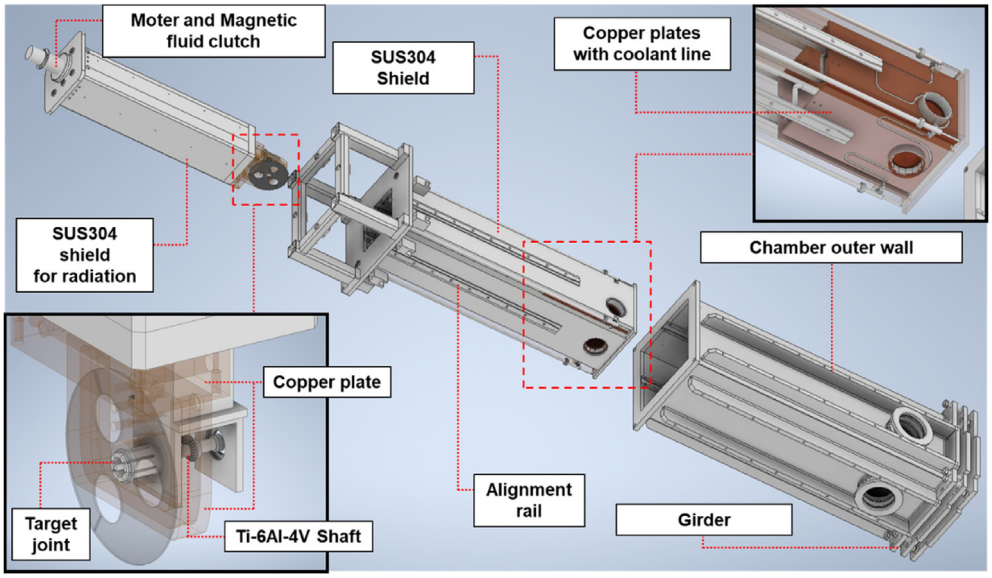

Fig. 11. Composition of target system.

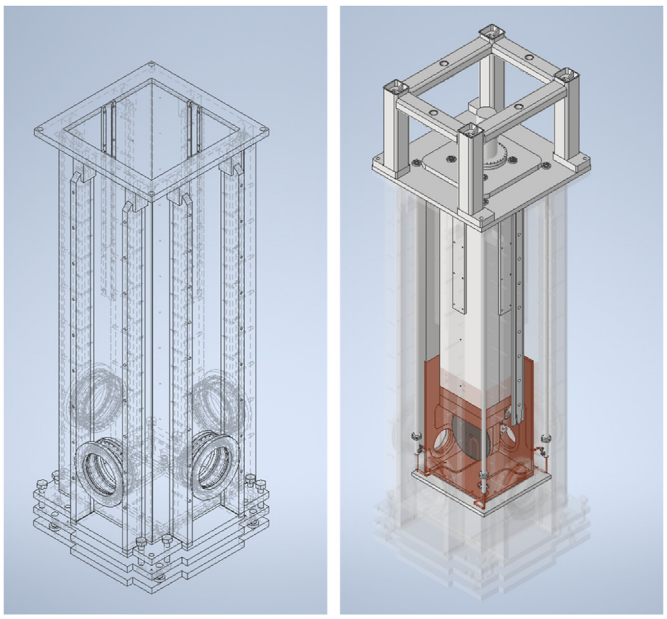

Fig. 12. Multiple ports in chamber (Left) and drawing of the target system (Right).

coefficient) was calculated using the Dittus–Boelter equation (2), where Dh is the hydraulic diameter, Re is the Reynolds number, Pr is the Prandtl number, and *Nu* is the Nusselt number [17]. It is valid when Pr is between 0.6 and 160, Re_{Dh} is higher than 10000, and L/D is higher than 10.

$$Nu_{Dh} = 0.023 Re_{Dh}^{0.8} Pr^{0.4} \quad (1)$$

The maximum temperature of the copper plate by the flow rates of the coolant obtained through ANSYS calculation is shown in Fig. 13.

In the absence of coolant, the temperature of the copper plate increased to 1215 °C. Fig. 13 shows that the temperature decreases rapidly until the flow velocity is 0.5 m/s, and then a gentle temperature difference is shown above 0.5 m/s. Moreover, the maximum temperature at this flow rate did not exceed the standard at the beginning of 60 °C. Therefore, the minimum flow rate of the coolant flowing through the 14 mm diameter copper cooling pipe was determined as 0.5 m/s.

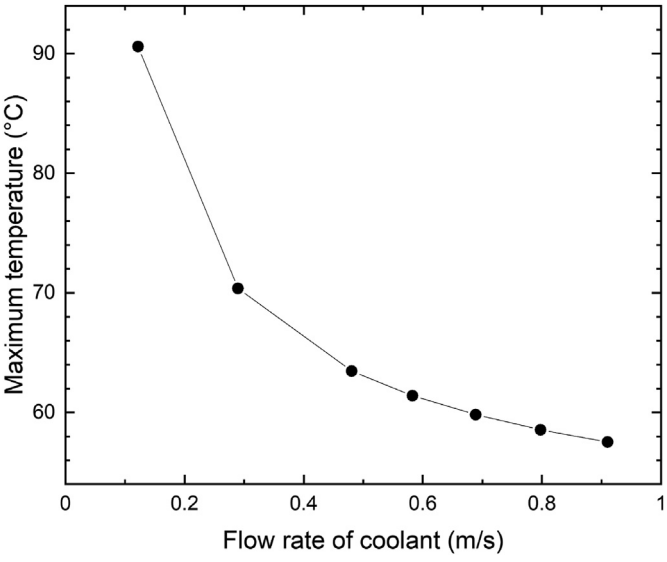

Fig. 13. The maximum temperature of the copper plate by flow rates of the coolant.

The thermal stress applied to the chamber was calculated for the determined flow rate, and it was verified that the stress did not exceed the yield strength of each material. The yield strength of the chamber components is shown in Table 5 below [18].

At that flow rate, the maximum stress of the part made of SUS304 is 119.88 MPa, and the maximum stress of the part made of copper is 49.967 MPa. Compared to the yield strength of each material, it can be judged to be sufficiently safe by comparing the yield strength of each material.

4. Summary and outlook

A target system for the muon facility in RAON has been designed and aims to start production within 2020. To obtain reliable simulation results, our Geant4 simulation results were compared with the data obtained by the PSI. From the comparison, it was evident that the expected surface muon yield is estimated to be 3.432 times lower than our simulation result with the QGSP_INCLXX model in order to obtain more realistic and conservative results. The target shape was determined to be a disk-shaped rotating target, which can induce the production of significantly many surface muons in thermally stable experiments. The suitable target width and radius to maximize the surface muon yield were obtained considering the mechanical strength and expected temperature when 100 kW proton beam collided. The target width was determined as 5 mm considering both the surface muon yield and requirements for structural strength of the target. The temperature calculations indicated that the maximum temperature would not exceed the temperature criterion when the outer radius of the target was 200 mm. The maximum temperature and the thermal stress with the determined target were 1482.7 °C and 0.3213 MPa, respectively, with a 100 kW proton beam. The maximum stress owing to temperature distribution was sufficiently low to guarantee safety during the replacement cycle of the target. Under this condition, the number of surface muons at the entrance of the beamline was 4.736×10^7 per second when the target was bombarded with a 40 kW proton beam, which is a sufficient surface muon yield to perform the μSR experiment; even when considering the loss owing to beam transport efficiency. The vacuum chamber was designed to maintain a vacuum for the operation of the designed target. The main considerations of target chamber design were as follows: stable vacuum for high doses and high heat during operation, ease of production, and alignment of the target. The final production design of the above target system will be completed within 2020, and manufacturing will begin immediately. The limitation of the designed target system is that no experiment has been conducted yet, but only simulations. However, the design has a sufficient safety margin and has been done conservatively. The manufactured target system will be installed at the RAON in the Sindong area near Daejeon-city in 2021 to carry out verification experiments for thermal calculation. An experiment to verify the surface muon yield will also be conducted with a beam profile monitoring system before the facility operation. Moreover, the target system has upgraded plans for operation with a 400 kW proton beam.

Table 5
Yield strength of the chamber components.

	SUS304	Oxygen-free Copper (C10100)
Yield strength (MPa)	205	69

Declaration of competing interest

The authors declare that they have no known competing financial interests or personal relationships that could have appeared to influence the work reported in this paper.

Acknowledgement

This work was supported by the Rare Isotope Science Project of the Institute for Basic Science funded by the Ministry of Science and ICT and the NRF of Korea (2013M7A1A1075764).

References

[1] C.D. Anderson, S.H. Neddermeyer, Phys. Rev. 50 (1936) 263.
[2] PSI-LMU, Laboratory for muon spin spectroscopy, Available online: https://www.psi.ch/lmu/. (Accessed 15 October 2020).
[3] J-PARC/MUSE, Available online: http://www.j-parc.jp/MatLife/en/index.html.
[4] RCNP–MuSIC, Available online: http://www.rcnp.osaka-u.ac.jp/RCNPhome/music/. (Accessed 1 November 2018).
[5] TRIUMF centre for molecular and materials science, Available online: http://cmms.triumf.ca/. (Accessed 15 October 2020).
[6] ISIS Muons, Available online: https://www.isis.stfc.ac.uk/Pages/Muons.aspx. (Accessed 1 November 2018).
[7] K. Pak, J. Park, Y.H. Kim, et al., J. Kor. Phys. Soc. 77 (2020) 438–442.
[8] CERN, Geant4—version 4.10.6.p01. http://geant4.cern.ch. (Accessed 15 October 2020).
[9] TOYO TANSO, Available online: http://www.toyotanso.co.jp/index_en. (Accessed 15 October 2020).
[10] W. Higemoto, R. Kadono, N. Kawamura, et al., Quantum Beam Sci 1 (2017) 11.
[11] A. Kurumada, T. Oku, K. Harada, et al., Carbon 35 (1997) 1157–1165.
[12] AZO MATERIALS homepage. https://www.azom.com/. (Accessed 15 October 2020).
[13] J.R. Haines, C.C. Tsai, Graphite Sublimation Tests for the Muon Collider/neutrino Factory Target Development Program, Oak Ridge National Laboratory, 2002. ORNL/TM–2002/27.
[14] J.B. Sohn, J.H. Lee, G.D. Kim, et al., J. Kor. Phys. Soc. 67 (2015) 1490.
[15] X. Los Alamos Scientific Laboratory Group, MCNP: a general Monte Carlo code for neutron and photon transport. https://mcnp.lanl.gov/. (Accessed 4 November 2019).
[16] F. Berg, L. Desorgher, A. Fuchs, W. Hajdas, Z. Hodge, P.R. Kettle, A. Knecht, R. Lüscher, A. Papa, G. Rutar, M. Wohlmuther, Physical Review Accelerators and Beams 19 (2016), 024701.
[17] F.W. Dittus, L.M.K. Boelter, Int. Commun. Heat Mass Tran. 12 (1985) 3–22.
[18] MatWeb, Available online: http://www.matweb.com/. (Accessed 4 November 2020).